Mountain formation by repeated, inhomogeneous crustal failure in a neutron star

A. D. Kerin[1] and A. Melatos[1,2]

[1] *School of Physics, University of Melbourne, Parkville, VIC 3010, Australia*
[2] *Australian Research Council Centre of Excellence for Gravitational Wave Discovery (OzGrav), University of Melbourne, Parkville, VIC 3010, Australia*

As a neutron star spins down mechanical strain accumulates in the solid crust up to and beyond the point of failure. To model the repeated macroscopic failure of the crust an idealised cellular automaton is developed, with nearest-neighbour interactions representing strain dissipation and redistribution, and including thermal losses. The probability distribution functions (PDFs) of the size and waiting times of failure events in the automaton are presented. The final failure event of a star's life occurs when the star spins down to $\approx (5 \pm 3)\%$ of its birth frequency with implications for transient events e.g. rotational glitches. In addition the automaton is able to predict the star's mass-quadrupole moment and gravitational wavestrain at all points in the star's life, with relevance to future gravitational wave surveys such as those carried out with the Laser Interferometer Gravitational Wave Observatory (LIGO).

Keywords: Asteroseismology – gravitational waves – stars: evolution – stars: neutron – stars: rotation

1. Introduction

The mechanical failure of the crust of a rotating neutron star, and the associated creation of mountains, has been suggested as a source of continuous gravitational waves,[1–3] and transient events such as rotational glitches[4,5] and fast radio bursts.[6] No such gravitational waves have been observed despite multiple recent searches,[7–13] but theoretical arguments exist that the first detection is close.[2] It should be noted that other reasonable explanations for transients have been suggested, e.g. superfluid vortices in the context of glitches.[14,15]

The macroscopic, tectonic process by which the crust fails and mountains form is unknown.[16,17] By analogy with the Earth, one expects crustal failure to involve large-scale, inhomogeneous elements such as fault lines, plates, subduction zones, stress zones, and so on, even though the tensile properties of a neutron star's crust are likely to be different to those of terrestrial rocks (and indeed are not understood completely at present). Modelling has primarily focused on the microphysics of crustal failure.[18–22] In particular Ref. 19 found local cracking does not occur due to the extreme pressure and the crust material fails globally. There have been some investigations into the evolution of the whole star as it evolves through a quasistatic sequence of elastic equilibria.[23,24,31] However, these do not consider the impact of the stick-slip dynamics of repeated local failures involving inhomogenous tectonic features, e.g. tectonic plates, which lead to history dependent outcomes.

Here we present a model of local mountain formation caused by mechanical failure of the crust on macroscopic scales driven by spin down. The model describes the tectonics of crustal failure through a cellular automaton, similar in spirit to the block-and-spring automata used to describe the far-from-equilibrium, stick-slip dynamics of terrestrial earthquakes.[25] Section 2 deals with how the crust deforms due to spin down, the consequent strain build up, and the effects of repeated local failures. Section 3 briefly presents some of the results of this model, in particular the probability distribution functions (PDFs) of the heat dissipated in failure events and the time between events. Section 4 presents the gravitational wavestrain over time as a function of the automaton parameters. For simplicity we do not consider a magnetic field, which is unlikely to be important in ordinary neutron stars (although this may not be true in magnetars).

This paper summarises the key aspects of the model and its output as developed in Ref. 26. This summary borrows heavily from the structure and content of Ref. 26. Among other things, Figs. 1 and 2 are reproduced from the latter reference.

2. Tectonics of Mountain Formation

2.1. *Global deformation due to spin down*

A neutron star is composed of a superfluid core and a solid crystalline crust.[21,22,27–30] Other components, e.g. transitional layers containing nuclear pasta at the crust-core interface,[16] are neglected here for simplicity.

As a neutron star spins down the balance of centrifugal and gravitational forces changes and so does the equilibrium figure of the crust. We use the method of Ref. 31 to model the secular deformation due to spin down, which in turn allows for the calculation of the mechanical strain at every point in the crust. In Ref. 27 Eqs. (3)-(8) define a vector which describes the change in the star's equilibrium figure due to spin down from which the mechanical strain can be calculated, see also Eqs. (1)-(7) in Ref. 26.

2.2. *Local microscopic failure*

We propose that the strain built up over the course of spin down causes the crust to fail locally when strained beyond breaking, and that some fraction of the energy released from the strained crystal lattice of the crust causes the centre of mass of the failed section to move radially outwards, creating a mountain.

Estimates of the breaking strain of neutron star crust material vary many orders of magnitude, e.g. Ref. 32 found a breaking strain of $\sim 10^{-5}$ and the more recent results of Ref. 19 instead found a breaking strain of ~ 0.1. We follow the results of Ref. 19 and consider a breaking strain in the range 0.075 to 0.11. Additionally Ref. 19 found that the material fails in a global manner, i.e. local cracks do not form, but the simulation volume is $\sim 10^{11}$ fm^3 and the macroscopic crust likely behaves differently (see Sec. 2.3 in this paper and Sec. 2.3 in Ref. 26).

When the crust fails it deforms plastically. When a material is deformed plastically a fraction of the plastic work done, β, is dissipated as heat. The value of β depends on a variety of factors such as the material, current strain, strain rate, and deformation history.[33–37] As per Ref. 35 terrestrial metals such as copper and steel have $0.75 \lesssim \beta \lesssim 0.95$, however such metals are unlikely to be good analogues for neutron star crust material. It is extremely difficult to calculate a realistic value of β and we do not attempt to do so. Instead we conservatively set $\beta = 0.9$, taking the position that the significant majority of the plastic work done is dissipated as heat.

2.3. *Repeated global failure: An automaton*

Ref. 19 found, using a direct simulation of nucleonic crystal (neutron star crust material), that the material fails in a global sense. Due to the extreme pressure local failure, i.e. cracking, is not observed. However the simulation volume is $\sim 10^{11}$ fm^3 and the macroscopic crust likely behaves differently, as noted in Sec. 2.2. In reality there are likely to be macroscopic features like seismic faults. To model these stick-slip and stress-relax dynamics[25] we create an automaton.

We divide the crust into N discrete cells; cells are indexed by i, with $0 \leq i < N$, and have position (r_i, θ_i, ϕ_i). The half-annular shape of the cells (dictated by assumed symmetry) and their coordinates are discussed in detail in Sec. 2.3 and Appendix A of Ref. 26. Each cell is assigned a breaking strain, σ_i, uniformly randomly between 0.075 and 0.11, informed by the stress-strain curve calculated in Ref. 19. Strain is greatest at the base of the crust, so the elastic potential energy density is greatest there too. As such the strain of each cell is evaluated at the base of the crust.

Over the course of spin down the strain of each cell, γ_i, increases. We define failure as when a cell has strain equal to or greater than its breaking strain, $\gamma_i \geq \sigma_i$. A failed volume of material is less able to support mechanical loads and so shifts the load to the neighbouring volume.[38] To model this we implement a nearest-neighbours interaction. Upon failure adjacent cells receive a fraction of the strain "lost" by the failed cell, with

$$\gamma_{i\pm1} \mapsto \gamma_{i\pm1} + \frac{1}{3}D(1-A)\gamma_i, \tag{1}$$

$$\gamma_{N-1-i} \mapsto \gamma_{N-1-i} + \frac{1}{3}D(1-A)\gamma_i, \tag{2}$$

where $0 \leq D \leq 1$ and $0 \leq A \leq 1$ are constants of the automaton, and cells indexed by $i = 0$ and $i = N-1$ are adjacent.[a] $(1-A)\gamma_i$ is the amount of strain "lost" by cell i upon failure. Some portion of the released strain, $D(1-A)\gamma_i$, is redistributed amongst cell i's nearest neighbours as per Eqs. (1) and (2). The remaining portion

[a]The cells closest to the North pole, $i = 0, N-1$, and South pole, $i = \lfloor N/2 \rfloor$ for N odd, or $i = N/2, N/2-1$ for N even, are adjacent to two cells not three. As such during strain redistribution Eq. (2) does not apply and Eq. (1) should be evaluated with a factor of 1/2 rather than 1/3.

of strain, $(1-D)(1-A)\gamma_i$, is converted into plastic work deforming the crust, i.e. moving cell i. After the strain of the failed cell's nearest neighbours is increased the failed cell's own strain is updated accordingly,

$$\gamma_i \mapsto A\gamma_i. \tag{3}$$

The quantity A is the fraction of strain a failed cell retains upon failure, and D is the fraction of strain released from the failed cell that is redistributed to the nearest neighbours. We call A and D the "dissipation" and "redistribution" parameters respectively.

In the failure process described above the crust is deformed plastically. The failed cell i is moved purely radially (θ_i and ϕ_i are unchanged) a distance Δr_i to model the plastic deformation,

$$r_i \mapsto r_i + \Delta r_i. \tag{4}$$

Δr_i is calculated by equating the energy associated with plastic deformation with the work done moving the cell against the gravitational-centrifugal potential a distance Δr_i. The potential is given by[31]

$$\Phi(\vec{r}) = -\pi G\rho_{\text{core}}\left[2R^2 - \frac{2r^2}{3} - \frac{4e^2r^2}{15}P_2(\cos\theta)\right], \tag{5}$$

where G is the gravitational constant, ρ_{core} is the density of the fluid core, and e is the eccentricity of the ellipse defined by the meridional cross-section of the star.

In general the mechanical potential energy U stored in a body of volume V under a strain γ is given by the strain-energy formula

$$\frac{\mu\gamma^2}{2} = \frac{U}{V}, \tag{6}$$

where μ is the shear modulus of the material. The mechanical potential energy density of a given cell i is then $\mu\gamma_i^2/2$. As described above if a given cell i with strain γ_i fails then the amount of strain that is converted into plastic work is $(1-A)(1-D)\gamma_i$. We calculate Δr_i from

$$\frac{\mu(1-\beta)}{2}[(1-A)(1-D)\gamma_i]^2 = \Delta r_i \rho_{\text{crust}} \left.\frac{d\Phi(\vec{r})}{dr}\right|_{\vec{r}=\vec{r}_i}, \tag{7}$$

where ρ_{crust} is the density of the crust, and β is the coefficient of thermal dissipation. As per Sec. 2.2 we take the conservative position of $\beta = 0.9$, i.e. we assume the significant majority of the plastic work done on the crust during failure is dissipated as heat.

The state of each cell in the automaton is described by five numbers $[r_i(t_n), \theta_i(t_n), \phi_i(t_n), \gamma_i(t_n), \sigma_i(t_n)]$, which are updated at each time-step. Here the i index refers to the cell index and t_n corresponds to the time-step. The initial shape of the star is a Maclaurin spheroid with eccentricity $e = 0.1$, a representative value.

The specific steps of the automaton are given:

(1) Choose the values of A and D.
(2) Initialise $[r_i(t_0), \theta_i(t_0), \phi_i(t_0)]$.
(3) Randomly assign each cell a breaking strain in the range $0.075 \leq \sigma_i \leq 0.11$, and set $\gamma_i = 0$.
(4) Using the method of Ref. 31 calculate the deformation vectors and increase the strain of each cell for a small spin down of $\delta\Omega$ and the fiducial values below in Sec. 2.4.
(5) If a cell i has $\gamma_i \geq \sigma_i$ then it undergoes failure.
    (a) Redistribute the strain of failed cell i to its nearest neighbours as per Eqs. (1) and (2) synchronously, i.e. all cells with $\gamma_i \geq \sigma_i$ are identified and fail simultaneously before Eqs. (1) and (2) are applied.
    (b) Move cell i radially as per Eqs. (4) and (7).
    (c) Decrease the strain in cell i as per Eq. (3).
    (d) Assign to cell i a new breaking strain, uniformly randomly in the range $0.075 \leq \sigma_i \leq 0.11$.
    (e) Repeat the steps (5)(a) to (5)(e) until $\gamma_i < \sigma_i$ for all $0 \leq i < N$.
(6) Decrease Ω by $\delta\Omega$.
(7) Repeat from step (4) until one has $\Omega \leq \delta\Omega$.

2.4. *Fiducial parameters*

The fiducial values used for this automaton are: $\mu = 2.4 \times 10^{29}$ Jm^{-3}, total radius $R = 10.5$ km, crust-core radius $R' = 9.5$ km, $\rho_{\rm core} = 6.38 \times 10^{17}$ kgm^{-3}, $\rho_{\rm crust} = 10^{17}$ kgm^{-3}, total stellar mass of 1.4 solar masses, $\Omega(0)/2\pi = 800$ Hz, and $\dot{\Omega}(0)/2\pi = -1 \times 10^{-8}$ Hzs^{-1}. For $A = D = 0.5$ and the above fiducial values the failure of a cell on the equator with $\sigma_i = 0.1$ leads to $\Delta r_i \approx 0.04$ mm. For the purpose of calculating the gravitational wavestrain we consider a star that is a distance $d = 1$ kpc away from the Earth.

In this automaton we set $N = 400$. The typical angular velocity step per automaton time-step is $\delta\Omega = (1.25 \times 10^{-4})\Omega(0)$. To convert $\Omega(t)$ into time t in what follows, we use $\Omega(t) = \Omega(0)(1 + t/\tau)^{-1/2}$ where $\tau = -\Omega(0)/2\dot{\Omega}(0) = 4 \times 10^{10}$ s, is the electromagnetic spin-down timescale.

3. Event Statistics

The automaton allows for the location of every part of the crust to be known at every point in time over the course of the star's life. Additionally the time, location, and energy of failure events are tracked. Numerous observables are studied as functions of t in Ref. 26. In Sec. 3.1 we focus on the PDF of event sizes. The PDF of the time between one event and the next one (the waiting time) and the age of the star at which tectonic activity ceases are presented in Sec. 3.2, and the correlation between event size and waiting time is presented in Sec. 3.3.

3.1. *Size PDF*

Mechanical failure of the crust has been linked to multiple types of transient events such as rotational glitches,[4,5] soft gamma-ray repeaters[22,39,40] and fast radio bursts.[6] Testable models of the transients' statistics, such as the automaton presented here, are needed to differentiate between crustal failure and other viable explanations of the transients e.g. superfluid vortices in the context of rotational glitches.[14,41–44]

In the upper panel of Fig. 1 we present the PDFs for the heat dissipated in an event, i.e. its size, given as ΔE. The left-hand side of Eq. (7) gives the amount of energy done as plastic work on the crust not lost as heat. Thus multiplying by $\beta/(1-\beta)$ gives the energy that is dissipated as heat in a failure event. The qualitative form of the PDF is similar across parameter space, a tight peak with a tail in increasing ΔE. Close to $A = D = 0$ events are largest with $\langle \Delta E \rangle \approx 5.4 \times 10^{36}$ J and the tail is most strongly suppressed; events with $\Delta E > \langle \Delta E \rangle$ are relatively less likely than in other regions of parameter space. Close to $A = D = 1$ events are smallest with $\langle \Delta E \rangle \approx 1.9 \times 10^{33}$ J and the tail is much more pronounced; events with $\Delta E > \langle \Delta E \rangle$ are relatively more likely than in other regions of parameter space. The decrease in $\langle \Delta E \rangle$ with increasing A and D follows from Eq. (7). The change in the tail comes from larger A and D more easily facilitating avalanches. More frequent avalanches means larger events are more frequent. For larger A cells remain close to critical after failure, and are thus more prone to fail when a neighbour does. For larger D the nearest-neighbours interaction is simply stronger.

3.2. *Waiting-time PDF*

We define the waiting time of an event, Δt, as the time between that event and the next one. In the lower panel of Fig. 1 we present the PDFs of waiting time for a variety of values of A and D. There is a steep rise for small Δt with an approximately exponential tail for high Δt, the probability density peaks at $\Delta t \approx 0.1\tau$. Recall τ is the spin-down timescale as defined in Sec. 2.4. The waiting-time PDF is approximately exponential, with the peak at $\Delta t \approx 0.1\tau$ an artifact of time discretisation. The frequency decrement, $\delta\Omega$, is constant. Correspondingly the time-steps are small early in the star's life and large later on. As such short waiting-time events are restricted to early in the star's life whereas long waiting-time events can happen throughout. In contrast to the PDF of event sizes the PDF of waiting times is unaffected by A or D. This is because the driver of events is the rate of strain build up, which is governed by spin down and unaffected by A or D.

In order for failure to occur at all we find that the star must be born with an initial rotational frequency $\gtrsim 750$ Hz, consistent with the results of Ref. 27. However once failure does occur, it continues until the star is near totally spun down, $\approx 5 \pm 3\%$ of the birth frequency, i.e. $t/\tau \approx 100$ to 2500. This is because the only way for strain to exit the system is through failure events, it otherwise continually builds up.

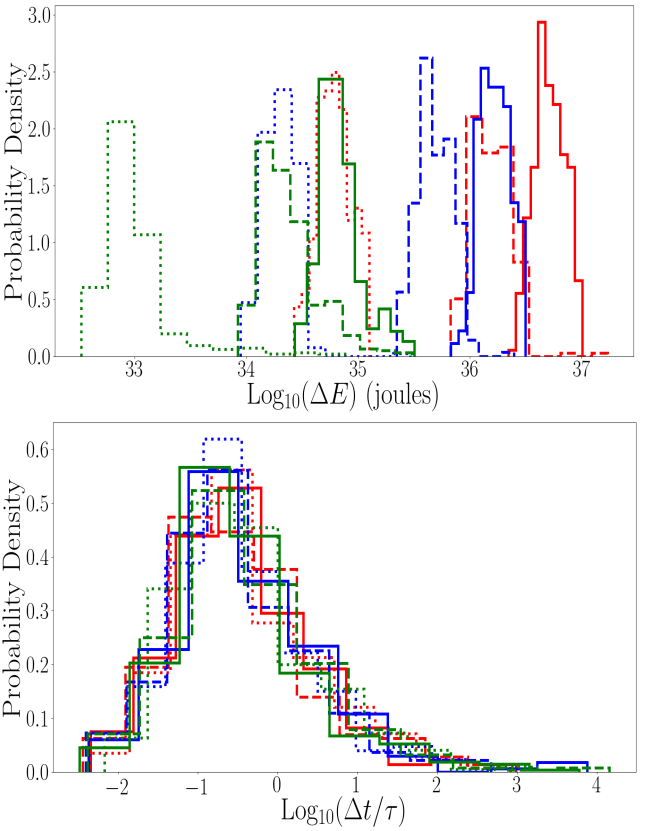

Fig. 1. Size PDFs, measured in joules, for a range of A and D (top panel). Waiting-time PDFs, measured in units of spin-down timescale, τ, for a range of A and D (bottom panel). In both panels red corresponds to $A = 0.1$, blue to $A = 0.5$ and green to $A = 0.9$. The solid lines correspond to $D = 0.1$, dashed to $D = 0.5$ and dotted to $D = 0.9$. Each PDF is constructed from all the events from five simulations. This figure is copied from Ref. 26.

3.3. *Size-waiting-time correlations*

Also of interest are the correlations between the size of an event and the waiting time (recall the waiting time is the time until the next event). We find that the Spearman rank coefficient is ≈ 0.3 uniformly across parameter space. On average larger events affect more of the crust and so, post-failure, cause a larger fraction of the crust to be further from failure, meaning that the average time until the next event is longer. However larger events do not necessarily affect more of the crust, due to the random breaking strains of cells, causing the correlation to be weak. Additionally it is possible for a large event to simply not involve the next-closest-to-failure cell and thus do nothing to delay the next event, further weakening the correlation.

4. Gravitational Radiation

Continuous gravitational waves are the subject of many recent, albeit unsuccessful, searches.[7–13] As such we are motivated to calculate the signal expected from possible sources. Here we consider an isolated spinning-down neutron star with mountains forming due to mechanical failure of the crust. Other potential sources of continuous waves include X-ray binaries[45] and accreting neutron stars.[46] In this model the location of every part of the crust, and the rotational frequency, is known for all of the star's life, so the gravitational wavestrain can be calculated at all times.

In Fig. 2 we plot the wavestrain over time from a neutron star. The two dynamical factors that determine the wavestrain are the changing failure-induced mass-quadrupole moment and the decaying rotational frequency, with $h_0 \propto Q\Omega(t)^2/d$, where h_0 is the gravitational wavestrain, Q is the mass-quadrupole moment, and d is the distance from Earth. At early times spin down is rapid, causing strain to accumulate quickly and many failures to occur, leading to a rapid increase in Q, thus causing the sharp initial rise in Fig. 2. As the star spins down $\dot{\Omega}(t)$ decreases, this slows the rate of mountain creation and causes Q to increase more slowly. At $t/\tau \approx 5$ to 10 the effect of increasing Q balances with the effect of decreasing $\Omega(t)$, causing the wavestrain reach its maximum value. After the peak in wavestrain the decreasing frequency leads to $h_0 \propto (1 + t/\tau)^{-1}$ for $t \gtrsim 10\tau$.

Similar to the size of events the wavestrain is largest near $A = D = 0$ peaking at $h_0 \approx 5 \times 10^{-28}$ and smallest near $A = D = 1$ peaking at $h_0 \approx 1.6 \times 10^{-31}$. Larger events create larger mountains and so lead to a greater waverstrain. Wavestrain reaches a maximum at $t/\tau \approx 5$ to 10, corresponding to $\Omega(t)/2\pi \approx 250$ to 320 Hz. There is no trend with A or D in when the wavestrain peaks. The timing of the peak

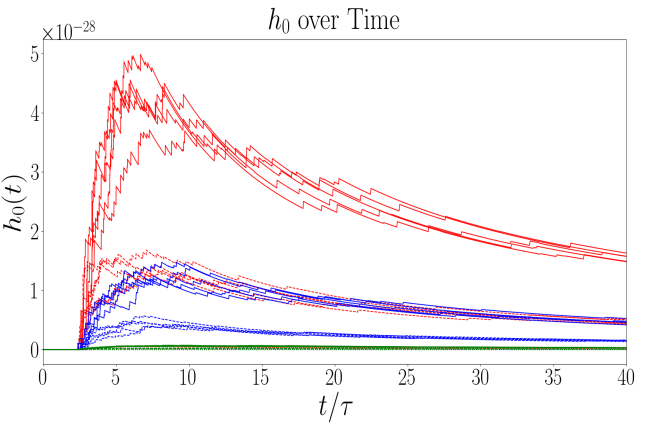

Fig. 2. Gravitational wavestrain, $h_0(t)$, as a function of time, t, in units of the spin-down timescale τ. Each line is the wavestrain of an individual run, of which there are five per value of (A, D). Red corresponds to $A = 0.1$, blue to $A = 0.5$ and green to $A = 0.9$. The solid lines correspond to $D = 0.1$, dashed to $D = 0.5$, dotted to $D = 0.9$. This figure is copied from Ref. 26.

is determined by the rate of events and spin down, neither of which is impacted by A or D.

It should be noted that spin down induced-failure is not the only potential source of mountains on neutron stars. Mountains may form on accreting stars[46] and r-mode oscillations may also lead to a detectable current-quadrupole gravitational wave signal.[47]

5. Conclusion

Electromagnetic spin down drives centrifugal crustal deformation and repeated crustal failure in rotation-powered pulsars. Crustal failure may be responsible for impulsive phenomena like rotational glitches.[4,5] It may also create mountains which lead to the continuous emission of gravitational radiation.[1–3] Molecular dynamics simulations reveal that the crust fails homogeneously, without cracking, under the high pressures on neutron stars.[19] However the simulations are conducted on picometre scales and cannot resolve inhomogeneities on macroscopic length scales (e.g. $\gtrsim 1$ m) such as tectonic plates, faults, and so on, which are seeded by dislocations and other impurities and grow under repeated failure. In this paper, we develop a phenomenological model in the form of a cellular automaton to capture - in a highly idealised form - some of the far-from-equilibrium physics of repeated failure.

We present an idealised cellular automaton to model the evolution of the crust as it both spins down secularly and deforms plastically due to mechanical failure. The secular deformation and strain build up are modelled using the method of Ref. 31. We make use of a nearest-neighbours interaction to model the redistribution and dissipation of strain and the plastic deformation following crustal failure, including the effects of thermal dissipation.

In this model the time, location and size of every failure event are known, as is position of every part of the crust at every point in time. This allows for a wide variety of observables to be predicted, e.g. total tectonic activity, rate of tectonic activity, and number of events. These observables, among others, are investigated in greater detail in Ref. 26. We find the ΔE PDF is qualitatively similar for all values of A and D, namely a tight peak with a tail in increasing ΔE. Events are largest near $A = D = 0$ with $\langle \Delta E \rangle \approx 5.4 \times 10^{36}$ J and smallest near $A = D = 1$ with $\langle \Delta E \rangle \approx 1.9 \times 10^{33}$ J. The gravitational wavestrain follows a similar pattern due to larger events creating larger mountains. The maximum emitted wavestrain in the star's life is greatest near $A = D = 0$ with $h_0 \approx 5 \times 10^{-28}$ and smallest near $A = D = 1$ with $h_0 \approx 1.6 \times 10^{-31}$. In contrast we find that the waiting-time PDF is insensitive to A and D.

The key predictions of this model are (i) in order for failure to occur at all the star must be born spinning $\gtrsim 750$ Hz, consistent with the results of Ref. 27, (ii) once the first failure has occurred failures will continue until $\Omega(t) \approx (0.05 \pm 0.03)\Omega(0)$, and (iii) there is a weak positive correlation (Spearman rank coefficient ≈ 0.3) between the size of an event and the time until the next one.

We plan to improve this calculation in future. Refs. 23 and 24 extend the formalism of Ref. 31. These extensions account for the stratification of the star i.e. they allow for the consideration of a star of multiple variously dense layers, rather than requiring a two component crust-core formulation, additionally they model perturbations from chemical equilibrium.

References

1. K. Riles, Gravitational waves: Sources, detectors and searches, *Progress in Particle and Nuclear Physics* **68**, 1 (2013).
2. G. Woan, M. Pitkin, B. Haskell, D. Jones and P. Lasky, Evidence for a minimum ellipticity in millisecond pulsars, *The Astrophysical Journal Letters* **863**, p. L40 (2018).
3. B. Reed, A. Delbel and C. Horowitz, Modeling the galactic neutron star population for use in continuous gravitational wave searches, *arXiv preprint arxiv:2104.007711* (2021).
4. M. Ruderman, Crust-breaking by neutron superfluids and the vela pulsar glitches, *The Astrophysical Journal* **203**, 213 (1976).
5. J. Middleditch, F. E. Marshall, Q. D. Wang, E. V. Gotthelf and W. Zhang, Predicting the starquakes in psr j0537–6910, *The Astrophysical Journal* **652**, p. 1531 (2006).
6. A. G. Suvorov and K. D. Kokkotas, Young magnetars with fracturing crusts as fast radio burst repeaters, *Monthly Notices of the Royal Astronomical Society* **488**, 5887 (2019).
7. B. Abbott, B. P, R. Abbott, T. Abbott, S. Abraham, F. Acernese, K. Ackley, C. Adams, R. X. Adhikari, V. B. Adya, C. Affeldt *et al.*, Narrow-band search for gravitational waves from known pulsars using the second ligo observing run, *Physical Review D* **99**, p. 122002 (2019).
8. B. Abbott, R. Abbott, T. Abbott, S. Abraham, F. Acernese, K. Ackley, C. Adams, R. Adhikari, V. Adya, C. Affeldt *et al.*, Directional limits on persistent gravitational waves using data from advanced ligo's first two observing runs, *Physical Review D* **100**, p. 062001 (2019).
9. B. Abbott, R. Abbott, T. Abbott, S. Abraham, F. Acernese, K. Ackley, C. Adams, R. Adhikari, V. Adya, C. Affeldt *et al.*, Search for gravitational waves from scorpius x-1 in the second advanced ligo observing run with an improved hidden markov model, *Physical Review D* **100**, p. 122002 (2019).
10. B. Abbott, R. Abbott, T. Abbott, S. Abraham, F. Acernese, K. Ackley, C. Adams, R. Adhikari, V. Adya, C. Affeldt *et al.*, Searches for continuous gravitational waves from 15 supernova remnants and fomalhaut b with advanced ligo, *The Astrophysical Journal* **875**, p. 122 (2019).
11. B. Abbott, R. Abbott, T. Abbott, S. Abraham, F. Acernese, K. Ackley, C. Adams, R. X. Adhikari, V. B. Adya, C. Affeldt *et al.*, Searches for gravitational waves from known pulsars at two harmonics in 2015–2017 ligo data, *The Astrophysical Journal* **879**, p. 10 (2019).
12. R. Abbott, T. Abbott, S. Abraham, F. Acernese, K. Ackley, A. Adams, C. Adams, R. Adhikari, V. Adya, C. Affeldt *et al.*, Gravitational-wave constraints on the equatorial ellipticity of millisecond pulsars, *The Astrophysical journal letters* **902**, p. L21 (2020).
13. M. A. Papa, J. Ming, E. V. Gotthelf, B. Allen, R. Prix, V. Dergachev, H.-B. Eggenstein, A. Singh and S. J. Zhu, Search for continuous gravitational waves from the

central compact objects in supernova remnants cassiopeia a, vela jr., and g347. 3–0.5, *The Astrophysical Journal* **897**, p. 22 (2020).
14. P. Anderson and N. Itoh, Pulsar glitches and restlessness as a hard superfluidity phenomenon, *Nature* **256**, 25 (1975).
15. L. Warszawski and A. Melatos, Gross–pitaevskii model of pulsar glitches, *Monthly Notices of the Royal Astronomical Society* **415**, 1611 (2011).
16. M. Caplan and C. Horowitz, Colloquium: Astromaterial science and nuclear pasta, *Reviews of Modern Physics* **89**, p. 041002 (2017).
17. F. Gittins, N. Andresson and D. Jones, Modelling neutron stars, *arXiv preprint arXiv:2009.12794* (2021).
18. C. Horowitz and J. Hughto, Molecular dynamics simulation of shear moduli for coulomb crystals, *arXiv preprint arXiv:0812.2650* (2008).
19. C. Horowitz and K. Kadau, Breaking strain of neutron star crust and gravitational waves, *Physical Review Letters* **102**, p. 191102 (2009).
20. A. Chugunov and C. Horowitz, Breaking stress of neutron star crust, *Monthly Notices of the Royal Astronomical Society: Letters* **407**, L54 (2010).
21. C. Horowitz, J. Hughto, A. Schneider and D. Berry, Neutron star crust and molecular dynamics simulation, *arXiv preprint arXiv:1109.5095* (2011).
22. D. Baiko and A. Chugunov, Breaking properties of neutron star crust, *Monthly Notices of the Royal Astronomical Society* **480**, 5511 (2018).
23. E. Giliberti, M. Antonelli, G. Cambiotti and P. Pizzochero, Incompressible analytical models for spinning-down pulsars, *Publications of the Astronomical Society of Australia* **36** (2019).
24. E. Giliberti, G. Cambiotti, M. Antonelli and P. Pizzochero, Modelling strains and stresses in continuously stratified rotating neutron stars, *Monthly Notices of the Royal Astronomical Society* **491**, 1064 (2020).
25. R. Burridge and L. Knopoff, Model and theoretical seismicity, *Bulletin of the seismological society of america* **57**, 341 (1967).
26. A. Kerin and A. Melatos, Mountain formation by repeared, inhomogeneous crustal failure in a neutron star, *Submitted to the Monthly Notices of the Royal Astronomical Society* (2021).
27. F. Fattoyev, C. Horowitz and H. Lu, Crust breaking and the limiting rotational frequency of neutron stars, *arXiv preprint arXiv:1804.04952* (2018).
28. A. I. Chugunov, Neutron star crust in voigt approximation: general symmetry of the stress–strain tensor and an universal estimate for the effective shear modulus, *Monthly Notices of the Royal Astronomical Society: Letters* **500**, L17 (2020).
29. A. Kozhberov and D. Yakovlev, Deformed crystals and torsional oscillations of neutron star crust, *Monthly Notices of the Royal Astronomical Society* **498**, 5149 (2020).
30. A. A. Kozhberov, Breaking stress of coulomb crystals in the neutron star crust, *arXiv preprint arXiv:2011.04397* (2020).
31. L. M. Franco, B. Link and R. I. Epstein, Quaking neutron stars, *The Astrophysical Journal* **543**, p. 987 (2000).
32. R. Smoluchowski, Frequency of pulsar starquakes, *Physical Review Letters* **24**, p. 923 (1970).
33. D. Rittel, On the conversion of plastic work to heat during high strain rate deformation of glassy polymers, *Mechanics of Materials* **31**, 131 (1999).
34. P. Rosakis, A. Rosakis, G. Ravichandran and J. Hodowany, A thermodynamic internal variable model for the partition of plastic work into heat and stored energy in metals, *Journal of the Mechanics and Physics of Solids* **48**, 581 (2000).

35. D. Macdougall, Determination of the plastic work converted to heat using radiometry, *Experimental mechanics* **40**, 298 (2000).
36. J. Hodowany, G. Ravichandran, A. Rosakis and P. Rosakis, Partition of plastic work into heat and stored energy in metals, *Experimental mechanics* **40**, 113 (2000).
37. G. Ravichandran, A. J. Rosakis, J. Hodowany and P. Rosakis, On the conversion of plastic work into heat during high-strain-rate deformation, in *AIP conference proceedings*, (1)2002.
38. R. V. R. Hertzberg and J. Hertberg, *Deformation and Fracture mechanics of engineering materials*, 5 edn. (John Wiley and Sons Inc, 2013).
39. D. Kaplan, S. Kulkarni, M. Van Kerkwijk, R. Rothschild, R. Lingenfelter, D. Marsden, R. Danner and T. Murakami, Hubble space telescope observations of sgr 0526–66: New constraints on accretion and magnetar models, *The Astrophysical Journal* **556**, p. 399 (2001).
40. K. Hurley, S. Boggs, D. Smith, R. Duncan, R. Lin, A. Zoglauer, S. Krucker, G. Hurford, H. Hudson, C. Wigger *et al.*, An exceptionally bright flare from sgr 1806–20 and the origins of short-duration γ-ray bursts, *Nature* **434**, 1098 (2005).
41. L. Warszawski and A. Melatos, Knock-on processes in superfluid vortex avalanches and pulsar glitch statistics, *Monthly Notices of the Royal Astronomical Society* **428**, 1911 (2013).
42. W. Fulgenzi, A. Melatos and B. Hughes, Radio pulsar glitches as a state-dependent poisson process, *Monthly Notices of the Royal Astronomical Society* **470**, 4307 (2017).
43. A. Melatos, G. Howitt and W. Fulgenzi, Size-waiting-time correlations in pulsar glitches, *The Astrophysical Journal* **863**, p. 196 (2018).
44. J. B. Carlin and A. Melatos, Autocorrelations in pulsar glitch waiting times and sizes, *Monthly Notices of the Royal Astronomical Society* **488**, 4890 (2019).
45. G. Ushomirsky, L. Bildsten and C. Cutler, Gravitational waves from low-mass x-ray binaries: A status report, in *AIP Conference Proceedings*, (1)2000.
46. G. Ushomirsky, C. Cutler and L. Bildsten, Deformations of accreting neutron star crusts and gravitational wave emission, *Monthly Notices of the Royal Astronomical Society* **319**, 902 (2000).
47. N. Andersson and K. D. Kokkotas, The r-mode instability in rotating neutron stars, *International Journal of Modern Physics D* **10**, 381 (2001).